Available online at www.sciencedirect.com
ScienceDirect
Acta Materialia 57 (2009) 5165–5173
Acta MATERIALIA
www.elsevier.com/locate/actamat

Stress relaxation and the structure size-dependence of plastic deformation in nanotwinned copper

Lei Lu [a,b,*], Ting Zhu [c], Yongfeng Shen [a], Ming Dao [b], K. Lu [a], Subra Suresh [b]

[a] Shenyang National Laboratory for Materials Science, Institute of Metal Research, Chinese Academy of Sciences, Shenyang 110016, China
[b] Department of Materials Science and Engineering, Massachusetts Institute of Technology, Cambridge, MA 02139, USA
[c] Woodruff School of Mechanical Engineering, Georgia Institute of Technology, Atlanta, GA 30332, USA

Received 10 March 2009; received in revised form 6 July 2009; accepted 10 July 2009
Available online 11 August 2009

Abstract

Stress-relaxation experiments were performed on nanotwinned Cu to characterize the twin size-dependence of the activation volume and mobile dislocation density. We find that the variation of activation volume as a function of twin lamellae thickness can be captured well by a Hall–Petch-type relation. This structure size-dependence is interpreted to arise from a transition of the rate-controlling mechanism from intra-twin to twin boundary-mediated processes with decreasing twin thickness. Furthermore, we find that the exhaustion rate of mobile dislocations reduces with decreasing twin thickness. Such a twin size-dependence is attributed to the increased strain-hardening rate associated with a high density of coherent twin boundaries. Our results demonstrate that twin boundary-mediated dislocation processes can effectively promote the strain hardening and preserve mobile dislocations, leading to ultrahigh strength while retaining ductility in nanotwinned Cu.

Keywords: Nanoscale twins; Stress relaxation; Activation volume; Mobile dislocation density; Plastic deformation kinetics

1. Introduction

Nanostructured metals are strong, but their high strength is achieved at the expense of ductility [1–3]. The low tensile ductility arises because of the limited extent of uniform plastic flow, causing a much earlier onset of necking compared to their coarse-grained counterparts. The strain localization in the neck region of the tensile specimens induces microscopic damage that rapidly progresses to final failure. It has been shown that the extent of uniform deformation in metals is controlled by the plastic flow characteristics of strain hardening and strain-rate sensitivity, both of which are generally governed by dislocation density and velocity [4–8]. From the Orowan equation [9], the plastic strain rate $\dot{\gamma}_p$ can be expressed as:

$$\dot{\gamma}_p = \rho_m v b, \tag{1}$$

where ρ_m is the mobile dislocation density, v the dislocation velocity, and b is the magnitude of the Burgers vector. In Eq. (1), the mobile dislocation density characterizes the system's memory of plastic deformation history, reflecting the effect of the structural evolution of dislocation on plastic deformation; dislocation velocity represents the instantaneous rate effect on plastic flow. These plastic deformation characteristics have been well studied in coarse-grained bulk metals and alloys [10]. However, our understanding of their influences on nanostructured materials is limited, due to the paucity of relevant experiments.

Nanotwinned Cu (nt-Cu), comprising a polycrystalline structure that is populated with nanoscale coherent growth twins, exhibits an unusual combination of ultrahigh tensile strength (~1 GPa yield strength) and relatively high tensile

* Corresponding author. Address: Shenyang National Laboratory for Materials Science, Institute of Metal Research, Chinese Academy of Sciences, Shenyang 110016, China. Fax: +86 24 23998660.
E-mail address: llu@imr.ac.cn (L. Lu).

1359-6454/$36.00
doi:10.1016/j.actamat.2009.07.018

ductility (~14% elongation-to-failure) [11–13]. The coherent twin boundary (TB) is a special kind of internal interface with low energy. It can serve as an effective sink and source of dislocations, as well as a barrier against dislocation transmission [3]. An increase in twin density with decreasing twin thickness can strengthen ultrafine-grained Cu, similar to the grain-size-dependent strengthening in nanocrystalline (nc) metals [7]. However, nt-Cu achieves very high strength without significantly compromising ductility.

The plastic deformation kinetics in nt-Cu samples has been investigated to shed light on the strength–ductility tradeoff. For example, the strain-rate sensitivity of flow stress and the activation volume have been measured to infer the rate-controlling deformation mechanisms. From a series of experiments, including constant loading rate tests in nanoindentation [14], constant strain rate tests in tension and tensile strain rate jump tests [15], we found increased strain-rate sensitivity and reduced activation volume with decreasing twin thickness. This trend is similar to the grain size effect in face-centered cubic (fcc) nc metals. However, while both nt-Cu and nc metals exhibited increased strain-hardening rates in the early stage of plastic deformation, the extent of strain hardening in nc metals is very limited, resulting in their poor ductility (a few per cent of elongation-to-failure) [3].

In addition to the strain-rate-controlled experiments, characterizing the transient stress-relaxation behavior is another effective approach for probing the kinetic rate effect, as well as the structural evolution of dislocations. It specifically enables us to separate the contributions to the plastic strain rate of mobile dislocation density and velocity so that the dynamic evolution of mobile dislocation density can be quantitatively characterized. However, only a few stress-relaxation experiments have been reported for nc metals and none for nt metals so far. Such experiments are difficult to perform mainly because of the limited ductility, early onset of necking and plastic instability in nc metals. Wang et al. [16] reported the stress-relaxation experiments for nc-Ni with an average grain size (d) of 30 nm. They studied the effects of grain size and temperature on the activation volumes and mobile dislocation densities, and attributed the dominant mechanism to the GB-mediated dislocation processes [17]. Dalla Torre et al. [18] studied electrodeposited (ED) nc-Ni with $d \approx 21$ nm and high pressure torsion (HPT) nc-Ni with $d \approx 105$ nm by stress-relaxation tests. The ED nc-Ni showed a decreased activation volume with increasing stress, while the HPT nc-Ni showed an opposite trend. Both groups reported a high exhaustion rate of mobile dislocations in nc-Ni that was correlated with the limited ductility and fast strain hardening in the early stage of plastic deformation [16].

In this paper, we report on an experimental study of the twin size-dependence of plastic deformation kinetics in nt-Cu by using a stress-relaxation experiment. The ability of nt-Cu to sustain considerable uniform plastic deformation ensures a systematic measurement of repeated relaxation transients. We obtain the apparent and physical activation volumes, as defined in Section 2, thereby separating the contributions of mobile dislocation density and dislocation velocity to the kinetic rate of plastic flow. The twin thickness effect on both the activation volume and mobile dislocation density has been studied. The results provide a mechanistic basis for understanding the cooperation and transition between the intra-twin and inter-twin deformation mechanisms, as well as the structure length-scale effects on strain hardening and the strength–ductility tradeoff.

2. Theoretical background

The shear stress τ in a plastically deforming metal is generally regarded as consisting of two components:

$$\tau = \tau_i(\gamma_p) + \tau^*(T, \dot{\gamma}_p), \tag{2}$$

where τ^* is the thermal component of the shear stress. This component accounts for the stress needed to overcome the short-range barrier responsible for the temperature T and plastic strain rate $\dot{\gamma}_p$ dependence of flow; τ_i is the athermal contribution to the flow stress, resulting from the long-range internal stress impeding plastic flow, the temperature dependence of which is weak and arising mainly due to the temperature effect on the shear modulus μ.

For the plastic flow controlled by thermally activated dislocation glide, the dislocation velocity is given by [10]:

$$v = f_0 \exp\left(-\frac{\Delta G(\tau^*)}{k_B T}\right), \tag{3}$$

where f_0 is a pre-exponential constant, ΔG the activation free energy needed to surmount obstacles, and k_B is the Boltzmann constant. The physical activation volume is conventionally defined as:

$$V^* \equiv -\left.\frac{d\Delta G(\tau^*)}{d\tau^*}\right|_T. \tag{4}$$

In repeated stress-relaxation tests, V^* can be extracted from consecutive relaxation transients. Specifically, as the applied stress increases from the end of relaxation 1 to the onset of relaxation 2 in a short period, as shown in Fig. 1b, it is reasonable to assume that the variation of mobile dislocation density, ρ_m, is negligibly small. It follows that according to Eq. (1), the plastic strain rate is dictated by the dislocation velocity given by Eq. (3), such that V^* can be determined by:

$$V^* = k_B T \frac{\ln(\dot{\gamma}_{i2}/\dot{\gamma}_{f1})}{\Delta\tau^*}. \tag{5}$$

where $\dot{\gamma}_{i2}$ and $\dot{\gamma}_{f1}$ are the shear strain rate at the onset of relaxation 2 and at the end of relaxation 1, respectively.

In a single stress-relaxation transient, the apparent activation volume V_a can be determined by fitting the stress-relaxation curve according to [10]:

$$\Delta\tau(t) = -\frac{k_B T}{V_a} \ln\left(1 + \frac{t}{c_r}\right), \tag{6}$$

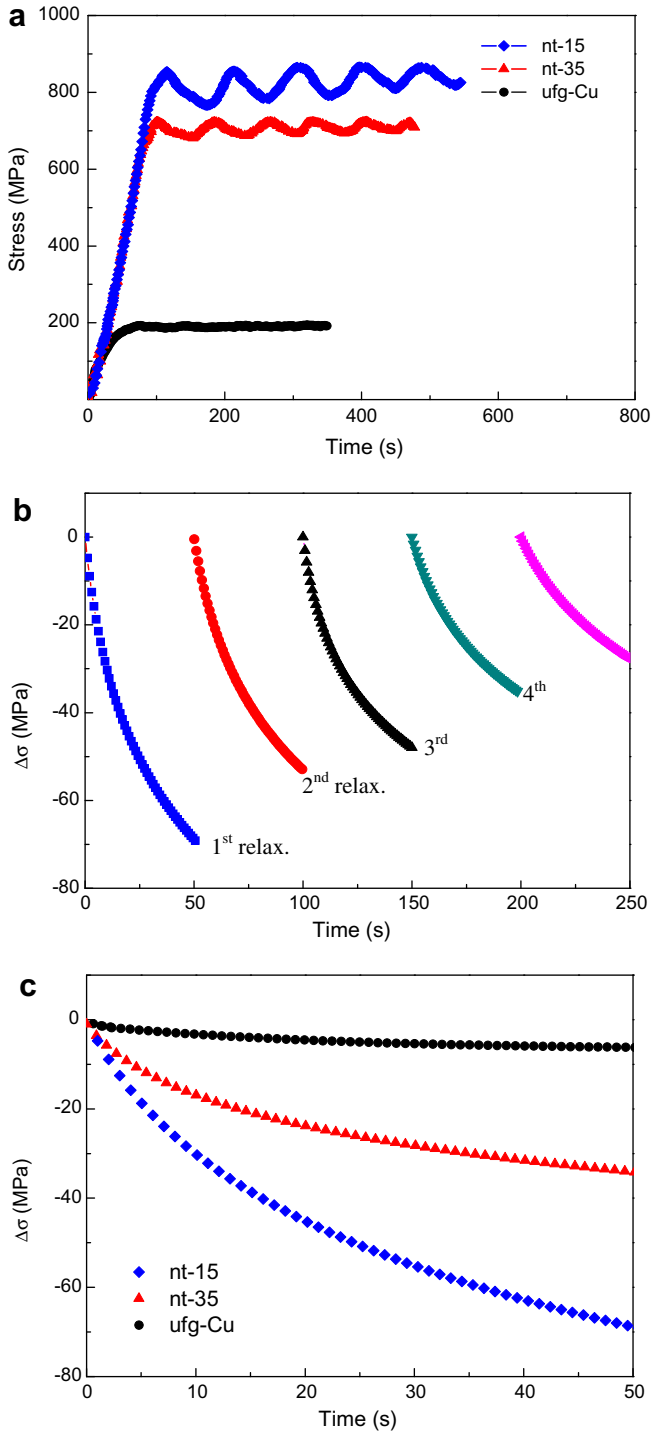

Fig. 1. (a) The stress–strain curves from the stress-relaxation experiments for nt-15, nt-35 and ufg-Cu without twins at room temperature; (b) a typical stress–relaxation series of nt-15 Cu; and (c) comparison of the stress decay $\Delta\tau$ during the first relaxation transient for the three Cu samples.

where $\Delta\tau$ is the stress drop at time t and c_r is the relaxation time constant.

It should be noted that the physical activation volume V^* is different from the apparent activation volume V_a. The former characterizes the stress sensitivity of dislocation velocity and the latter additionally incorporates the influence of mobile dislocation density. As a result, V^* is more directly linked to the dislocation processes that are rate-controlling. Generally, $\Omega \equiv V_a/V^* \geqslant 1$.

Combining Eqs. (3) and (4), one can relate the dislocation velocity v at time t to the initial dislocation velocity v_0 at $t = 0$ by:

$$v = v_0 \exp\left(\frac{\Delta\tau^* \cdot V^*}{k_B T}\right), \tag{7}$$

where $\Delta\tau^*$ is the change of τ^* from time $t = 0$ to time t; $\Delta\tau^* < 0$ in a typical stress transient. It is usually assumed that the mobile dislocation density ρ_m and the dislocation velocity v are related by an empirical power law:

$$\frac{\rho_m}{\rho_{m_0}} = \left(\frac{v}{v_0}\right)^{\beta}. \tag{8}$$

Based on Eqs. (1)–(8), it can be shown [10]:

$$\frac{\rho_m}{\rho_{m_0}} = \left(\frac{c_r}{t + c_r}\right)^{\frac{\beta}{1+\beta}}, \tag{9}$$

where ρ_{m_0} is the dislocation density at the start of the transient, and β is a dimensionless immobilization parameter:

$$\beta = \frac{\Omega}{1 + K/M} - 1. \tag{10}$$

Here, K is the strain-hardening coefficient, $\dot{\tau} = K\dot{\gamma}_p$ and M is the stiffness of the specimen–machine system [19,20]. The measured values of β are typically in the range of 0–1, as shown later in Table 1. Eq. (7) indicates that v is smaller than v_0 because $\Delta\tau^* < 0$. It follows that, according to Eqs. (8) and (9), the larger the value of β, the smaller the ratio, ρ_m/ρ_{m_0}, and the higher the exhaustion rate of mobile dislocation density. At another limit, Eq. (10) indicates that β approaches zero when $\Omega \approx 1$ and $K/M \ll 1$; this gives $\rho_m/\rho_{m_0} \approx 1$, corresponding to a low rate of mobile dislocation exhaustion.

While the activation volume and mobile dislocation density are defined in terms of the shear stress, the stress-relaxation experiment is generally performed in uniaxial tension. Invoking the von Mises yield criterion, the shear and normal stresses can be related by $\tau = \sigma/\sqrt{3}$. Correspondingly, the shear strain rate is related to the normal strain rate by $\dot{\gamma} = \sqrt{3}\dot{\varepsilon}$. This ensures the same work rate between shear and tension, i.e. $\tau\dot{\gamma} = \sigma\dot{\varepsilon}$.

3. Experimental

High-purity Cu foils with different densities of nanoscale growth twins were synthesized by means of pulsed electrodeposition from an electrolyte of $CuSO_4$ [14,15]. The foil has an in-plane dimension of 20 mm × 10 mm, and is about 100 μm thick. The density is 8.93 ± 0.03 g cm^{-3}. Chemical analysis indicated that the purity of as-deposited Cu is better than 99.998 at.% with a sulfur content less than 8 ppm, and oxygen and hydrogen concentrations less than

Table 1
Comparison of plastic flow parameters for the nt-Cu and ufg-Cu: yield strength σ_y, ductility (elongation-to-failure) δ, apparent activation volume V_a, physical activation volume V^*, the ratio $\Omega = V_a/V^*$, relaxation time constant c_r, strain-hardening coefficient K, immobilization parameter β, mobile dislocation density ρ_m at time t and ρ_{m_0} at $t = 0$.

Sample	σ_y (MPa)	δ (%)	$V_a b^3$	$V^* b^3$	Ω	c_r	K (MPa)	β	ρ_m/ρ_{m_0}	Relax no.
nt-15	830	14	20.7	16	1.290	2.351	10,000	0.057	0.85	1st
			20	15.7	1.275	2.793	8000	0.074	0.82	2nd
			19	15	1.266	2.966	8000	0.080	0.74	3rd
nt-35	660	5	36	30	1.186	3.521	3600	0.1	0.78	1st
ufg-Cu	200	15	350	309	1.128	1.10	700	0.128	0.641	1st

20 and 15 ppm, respectively. By modifying the pulsed electrodeposition parameters, a series of Cu specimens were obtained with similar grain size but different twin densities.

The as-deposited nt-Cu sample has roughly equiaxed grains with an average size of 400–600 nm. The structures of these specimens have been characterized systematically in our earlier studies on the same batch of materials [11,14,21]. The high density of TBs, which were introduced spontaneously inside each grain during the pulsed electrodeposition process, divides the ultrafine-grained crystals into nanometer-thick twin/matrix lamellar structures. Statistical measurements showed that the average thickness between adjacent TBs, λ, is approximately 15 ± 6 nm (hereafter referred to as nt-15) and 35 ± 7 nm (nt-35) in the $\langle 1\,1\,0 \rangle$ beam direction from plan-view transmission electron microscopy (TEM) observations. The length of the twin lamellae is roughly the same as the grain size. In addition, ultrafine-grained Cu with twin-free polycrystalline ensemble (hereafter referred to as ufg-Cu) is produced from the same electrolyte by direct current electrodeposition. No evident growth twin is observed in as-deposited ufg-Cu samples, whereas dislocations are present both inside grains and near GBs. Microstructural characterizations of both the as-deposited and deformed samples were performed in a transmission electron microscope (JEM 2010, JEOL Ltd., Japan) operated at 200 kV. Details of the TEM sample preparation can be found in Ref. [14].

Tensile specimens with a gauge length of 4 mm and a width of 2 mm were cut by electrodischarge machining. They were first mechanically polished from the deposited side with silicon carbide papers (1200–2000 grit), and then electrolytically polished to a mirror finish with an electrolyte consisting of 23% alcohol, 23% phosphorus acid, 5% isopropyl-alcohol and 49% deionized water (in vol.%). The final sample thickness after electropolishing is about 20 ± 5 μm, as measured by a Leica MPS 30 optical microscope (Leica Microsystems Inc., Wetzlar, Germany). A contactless MTS LX300 Laser extensometer (MTS Systems Corporation, Eden Prairie, MN, USA) was used to calibrate and measure the plastic strain during loading.

Stress-relaxation tests were performed by using a Tytron 250 Microforce Testing System (MTS System Corporation, Eden Prairie, MN, USA) at room temperature (approximately 20 °C and 50% relative humidity). The sample was initially strained to 1% at a strain rate of $6 \times 10^{-4}\ s^{-1}$, and then the cross-head was stopped and the stress was recorded as a function of time. After the first relaxation over an interval of 50 s, the specimen was reloaded to the same stress level as the beginning of the previous cycle for the next relaxation. In order to obtain reproducible experimental results, the stress relaxations of each sample were carried out at least five times.

4. Results

Fig. 1a shows repeated stress relaxations for nt-Cu with three different TB densities. The nt-15 sample exhibits the most significant stress drop $\Delta\sigma$ in each relaxation cycle. In contrast, $\Delta\sigma$ is very small in the twin-free ufg-Cu. Typical stress-relaxation transients for nt-15 are shown in Fig. 1b, where the change in stress at the onset of each relaxation cycle is taken as zero. In Fig. 1c, we compare stress transients in the first relaxation cycle (50 s). The stress drops for nt-15 and nt-35 are 70 and 37 MPa, respectively, while it is only 6 MPa for ufg-Cu.

The apparent activation volume V_a is determined by fitting σ vs. t according to Eq. (6). Fig. 2 shows the fitting curve (solid line) of the first relaxation cycle for nt-15, giving $V_a \approx 21b^3$ ($b = 0.265$ nm for Cu). Fig. 3 shows V_a fitted from repeated relaxation cycles, which varies between $21b^3$

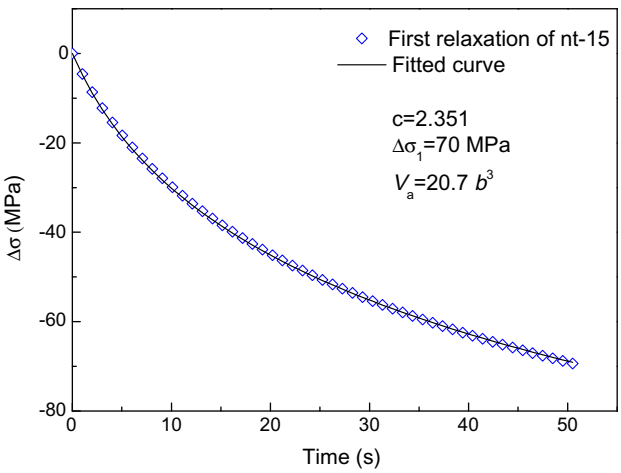

Fig. 2. Fitting of the experimental stress–relaxation curve for nt-15 Cu based on Eq. (6). V_a, apparent activation volume; c_r, relaxation time constant.

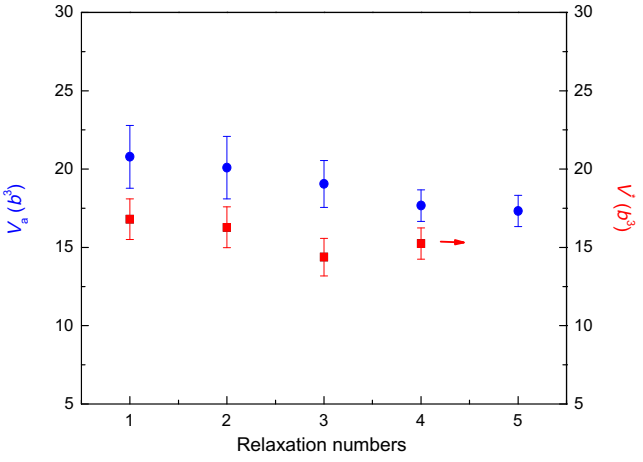

Fig. 3. The apparent activation volume V_a and physical activation volume V^* for different relaxation cycles of nt-15 Cu.

and $17b^3$ for nt-15. In Fig. 3, we also plot the physical activation volumes V^* determined from consecutive relaxation cycles for nt-15 based on Eq. (5), $V^* \approx 16b^3$, slightly lower than $V_a \approx 21b^3$. Both V_a and V^* decrease slightly with increasing number of cycles. Note that for nt-15, both V_a and V^* from the present stress-relaxation experiments are close to those from the strain rate jump tensile tests and nanoindentation tests ($12–22b^3$) [14,15], but differ from the activation volume (about $100–1000b^3$) in coarse-grained Cu by two orders of magnitude [22]. We also find that both V_a and V^* increase with twin thickness λ. For example, for ufg-Cu, they are $350b^3$ and $309b^3$, respectively, both of which are about 20 times higher than those for nt-15 (listed in Table 1).

As shown in Fig. 4, mobile dislocation density ρ_m/ρ_{m_0} is less than unity for both nt- and ufg-Cu, indicating the exhaustion of mobile dislocations with time during stress relaxation. The higher the twin density, the larger the value

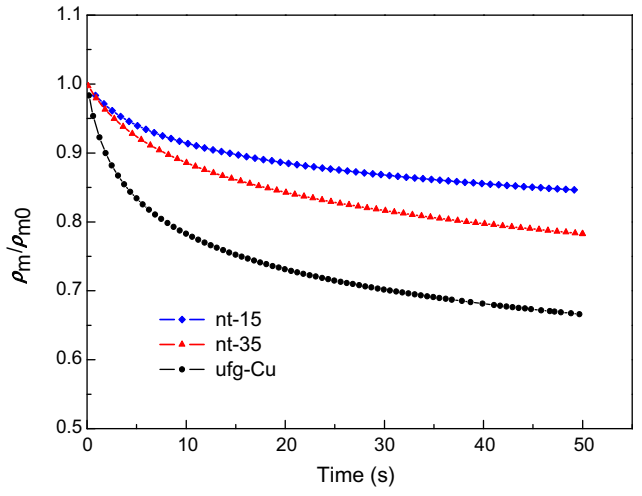

Fig. 4. Comparison of the evolution of mobile dislocation densities in the nt-15, nt-35 and ufg-Cu without twins during the first relaxation cycle (50 s).

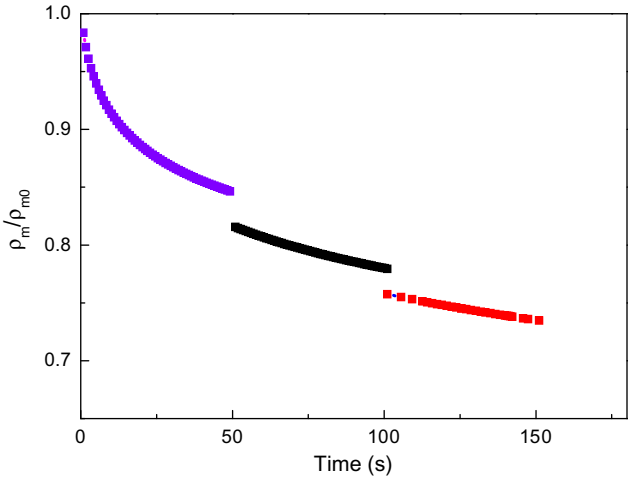

Fig. 5. Evolution of mobile dislocation density for nt-15 Cu during the first three relaxation cycles.

of ρ_m/ρ_{m_0}. For nt-15, ρ_m/ρ_{m_0} decreases to about 85% at the end of the first cycle ($t = 50$ s), implying a large portion of mobile dislocations remaining in the specimen. ρ_m/ρ_{m_0} decreases to 78% in nt-35, and is only 64% in ufg-Cu. A large value of ρ_m/ρ_{m_0} can be attributed to either a lower rate of annihilation or a higher rate of nucleation of mobile dislocations, or both, as analyzed in detail in Section 5.2. Fig. 5 shows the evolution of ρ_m/ρ_{m_0} for nt-15 during the first three cycles. The exhaustion rate of ρ_m decreases with increasing number of cycles. After three cycles, $\rho_m/\rho_{m_0} = 74\%$.

5. Discussion

5.1. Dependence of activation volume and deformation mechanisms on twin thickness

The activation volume is an effective kinetic signature of rate-controlling deformation mechanisms [23]. In coarse-grained fcc metals, a typical rate-determining process, such as the intersection of forest dislocations, gives a large activation volume of the order of several hundred to a few thousand b^3 [22,24]. At another extreme, GB sliding or GB diffusion mediated creep (Coble creep) gives a small activation volume of less than $1b^3$. When the activation volume is between $1b^3$ and $100b^3$, the rate process typically involves cross-slip or dislocation nucleation; the activation of either process requires a high local stress at the GPa level, so that the stress work ($\tau^* V^*$) associated with a relatively small activation volume can lower the effective energy barrier to a level sufficient to initiate the dislocation process within the timescale (seconds to minutes) of experimental measurements [25].

For the ufg-Cu without twins, the grain size is in the sub-micrometer range. The measured activation volumes are about $350b^3$, comparable to the literature data for coarse-grained Cu. This suggests that their rate-controlling mechanisms should be the same, primarily involving the intersection of forest dislocations in the bulk. For the

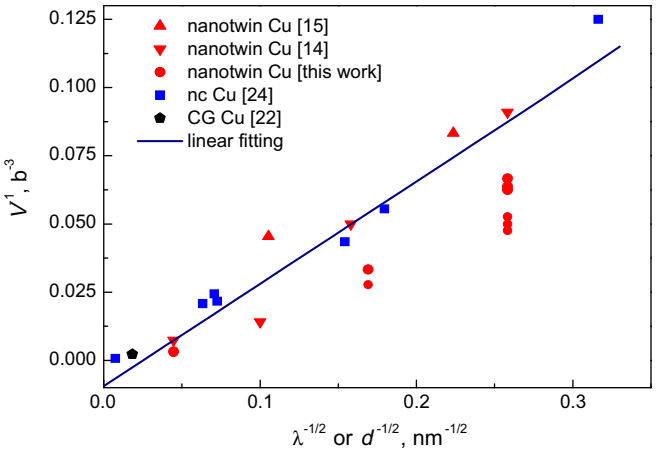

Fig. 6. Fitting of the experimental data of activation volume V^{-1} vs. twin thickness $\lambda^{-1/2}$ for nt-Cu (red symbols) based on Eq. (11), revealing a H–P-type size-dependence of activation volume. The data are collected from the strain rate jump test [15], nanoindentation test [14] and the stress–relaxation test in this work. For comparison, the rate sensitivity and activation volume are also shown as a function of $d^{-1/2}$ for nc-Cu (blue symbols) [26]. (For interpretation of the references to colour in this figure legend, the reader is referred to the web version of this article.)

ufg-Cu with a very high density of nanoscale twins, the activation volumes are much lower, e.g., $15b^3$–$20b^3$ in the case of nt-15 Cu. Computer simulations by atomistic reaction pathway calculations have shown that the associated rate processes involve dislocation cross-slip at the twin interface via the processes of dislocation accumulation, desorption and transmission [6]. It is interesting to note that the activation volumes in nt- and nc-Cu samples are comparable in magnitude when the twin thickness λ of nt-Cu is similar to the grain size d of nc-Cu, as shown in Fig. 6 and Table 2 [26].

Previously, the grain-size-dependence of activation volume has been studied for fcc metals by Conrad [24,27], Armstrong and Rodriguez [28], and Asaro and Suresh [29]. It was proposed that the intersection of dislocations in the bulk is the rate-controlling mechanism in coarse-grained metals, and the GB-mediated dislocation mechanism dominates when d is in the range of 10–100 nm. Between the two limits, a Hall–Petch (H–P)-type relation of the grain-size dependent activation volume was derived based on a dislocation pile-up model [27]. This H–P relation has been verified by the experimental data [28].

The atomic processes are different when impinging dislocations react with GBs and TBs because of their structure differences [3]. However, the size-dependence of activation volume in the nt system should be captured well by the H–P-type relation. This is because the essence of the dislocation pile-up model is to bring out the length-scale effects by invoking the size-mediated number of dislocations in the pile-up, $n(d)$ or $n(\lambda)$. As shown by Eqs. (2) and (3) in Conrad [27], $n(d)$ is a magnification factor that connects the applied stress and the local concentrated stress acting on the rate-determining processes at the GBs. Considering that the functional form of $n(d)$ and $n(\lambda)$ is independent of the nature of GB and TB in the pile-up model, we generalize the H–P-type relation of activation volume to include both the GB and TB effects:

$$\frac{1}{V}=\frac{1}{V_0^*}+\left[\frac{k_{\mathrm{GB}}}{2m\tau_c V_{\mathrm{GB}}^*}\right]d^{-1/2}+\left[\frac{k_{\mathrm{TB}}}{2m\tau_c V_{\mathrm{TB}}^*}\right]\lambda^{-1/2}, \tag{11}$$

where V is the activation volume of the specimen, V_0^* the activation volume associated with the intra-grain or intra-twin dislocation mechanism, i.e. intersection of lattice dislocations, and V_{GB}^* and V_{TB}^* are the activation volumes associated with the GB- and TB-mediated mechanisms, respectively. In Eq. (11), m is the Taylor factor ($m \approx 3.1$), and the constant k and the local shear resistance τ_{GB}^c or τ_{TB}^c are determined from the classic H–P model of dislocation pile-up. Considering that the measured tensile yield strengths for nt-Cu vary with twin thickness λ in the same manner as d for nc-Cu [11], we approximate $V_{\mathrm{GB}}^* = V_{\mathrm{TB}}^* = 25b^3$ and $k_{\mathrm{TB}} = k_{\mathrm{GB}} = 5.0\ \mathrm{MPa\ mm^{-1/2}}$ ($\tau_c = 450$ MPa, and the shear modulus $G = 30.5$ GPa). Using these data, V was predicted from Eq. (11) for nt-Cu with an average grain size of 500 nm and different twin thicknesses, as shown in the last row in Table 2. Fig. 6 and Table 2 show that the prediction (solid line) matches well with experimentally measured trends and values from this work and previous studies [6,14,15,26]. Note that for the ease of comparison with the literature data, here we did not distinguish the apparent and physical activation volumes as defined in Section 2, considering that their measured values are close and the data reported in the literature generally did not dis-

Table 2
Comparison between experimental measurements and the modeling prediction of strain-rate sensitivity and activation volume as a function of twin thickness.

	Twin thickness, λ (nm)				Ref.
	15	35	100	Twin-free	
m (exp, NI)	0.036 ± 0.009	0.025 ± 0.009	–	0.005	[14]
m (exp, jump test)	0.035–0.046	–	0.015–0.02	0.005	[15]
V (exp, NI)	$12b^3$–$15b^3$	$16b^3$	$22b^3$–$37b^3$	$135b^3$	[14]
V (exp, jump)	$9b^3$–$12b^3$	–	$22b^3$–$28b^3$	–	[15]
V (exp, relaxation)	$15b^3$–$21b^3$	$30 \sim 36b^3$	–	$309b^3$–$350b^3$	This work
V (atomistic calculated)	$24b^3$–$44b^3$	–	–		[6]
V (predicted from Eq. (11))	$19b^3$	$27b^3$	$40b^3$	$130b^3$	This work

tinguish between the apparent and physical activation volumes.

The twin-thickness dependence of activation volume shown in Fig. 6, along with its agreement with the dislocation pile-up model of Eq. (11), suggests a size-dependent transition of the rate-controlling mechanism from the intra-twin to inter-twin processes with decreasing twin thickness. TEM observations have revealed both the intra-twin to inter-twin processes. Fig. 7a shows an as-deposited specimen containing few lattice and TB dislocations. Fig. 7b shows dislocation structures in a deformed sample. In thin twins, a large amount of dislocation debris accumulates near TBs (see the white rectangle B in Fig. 7b), and the severely strained TBs contain a high density of boundary dislocations. High-resolution TEM observation identified that most of these boundary dislocations are Shockley partial dislocations [30]. In contrast, in wide twins a number of lattice dislocations and dislocation networks are stored inside lamellae (see the white rectangle A in Fig. 7b). Here we emphasize that both the intra-twin and inter-twin processes generally coexist in a TEM snapshot. By using the H–P-type relation of Eq. (11), we are able to include contributions to the size-dependent overall activation volume (and strain-rate sensitivity) from both intra-twin and inter-twin processes, each of which has a size-independent activation volume (V_0^* vs. V_{GB}^* or V_{TB}^*).

The above study of activation volumes provides mechanistic insights into the active rate mechanisms in plastic flow. Besides the rate-limiting effect, these dislocation processes can influence strain hardening and thus the strength–ductility tradeoff through, for example, mobile dislocation density, as detailed in Section 5.2. Furthermore, the complex dislocation configurations shown in Fig. 7 suggest that in general both the intra- and inter-twin mechanisms coevolve with deformation, and should contribute to strain hardening in a cooperative manner. Recent two-dimensional [30] and three-dimensional [31] crystal plasticity simulations of nt-Cu confirmed that, only by integrating these cooperative deformation mechanisms instead of exclusively considering the intra- or inter-twin mediated mechanism, can a reasonable correlation between the predictions of computational models and experimental results be achieved in terms of the size-dependent trends of strength, rate sensitivity and ductility.

5.2. Mobile dislocation density and strain hardening

An analysis of mobile dislocation density during stress relaxation can elucidate how the dynamically evolved dislocation structures influence the macroscopic deformation characteristics of strength, ductility and strain hardening. Dalla Torre et al. [18] showed that in coarse-grained Ni, ρ_m/ρ_{m_0} increases with stress, but in nc-Ni, ρ_m/ρ_{m_0} decreases as the applied stress increases. They attributed this grain size effect to different rate-controlling processes, i.e. dislocation multiplication in coarse-grained materials and dislocation exhaustion in nanocrystals. Wang et al. [16] measured the sharply decreased ρ_m/ρ_{m_0} in the initial stage of relaxation for nc-Ni. The high rate of mobile dislocation exhaustion was related to the ready availability of sources near the random GBs where dislocations can nucleate readily. But these GB sources are not regenerative and can be used up quickly upon straining, causing a rapid decay of the exhaustion rate of mobile dislocations [32]. Furthermore, they showed that as d deceases, ρ_m/ρ_{m_0} in nc-Ni reduces to about 0.1 at the end of the relaxation transient, much lower compared to 0.8 in coarse-grained Ni.

Fig. 4 shows that for nt-Cu an increase in the twin density can lower the exhaustion rate of mobile dislocations, creating a length-scale effect opposite to that on the

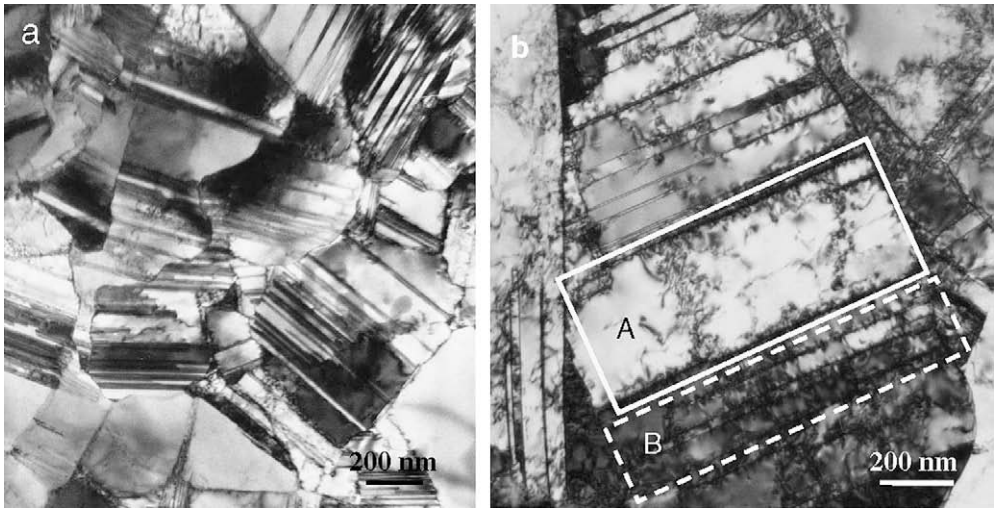

Fig. 7. TEM images of nt-15 Cu. (a) As-deposited sample showing that coherent TBs are initially straight and defect-free. (b) Sample after the stress–relaxation test showing the dislocation accumulation at TBs (as shown in rectangle B), as well as dislocation tangles and networks within the wide twin lamellae (as shown in rectangle A).

stress-relaxation rate (see Fig. 1c). Moreover, at the end of the first stress-relaxation cycle, ρ_m/ρ_{m_0} is about 0.85 in nt-15, much higher than that in nc-Ni (about 0.1). This result suggests that compared to GBs, TBs can more effectively preserve mobile dislocations.

The above results of the twin size effect, as well as the influences of TB vs. GB on ρ_m/ρ_{m_0}, can be understood by considering the TB-mediated slip transfer reactions. The crystallographic features of dislocation–TB interactions have been studied by Mahajan and his coworkers [33–35]. Recent research has focused on slip transfer reactions in nanoscale growth twins [36,37]. These studies show that interactions between dislocations with a Σ3 coherent TB in nt-Cu may result in glissile dislocations at the TB (i.e. twinning partials), sessile dislocations or locks at the TB, and/or outgoing dislocations or stacking faults in the neighboring twin layer, depending upon the nature of incoming dislocations. In Fig. 7, we compare dislocation microstructures before and after stress relaxation. Fig. 7a shows that in the as-deposited sample, coherent TBs are extremely "clean" and nearly dislocation-free, and thus they can readily trap and absorb lattice dislocations. The accumulated dislocations on TBs can remain mobile because of boundary coherency, so that they can easily glide along TBs to accommodate subsequent absorption and sustain plastic flow. This slip transfer of mobile dislocations at the coherent TBs is distinctly different from that at general high-angle GBs where dislocation glide is usually limited because of boundary incoherency, leading to a high rate of mobile dislocation exhaustion.

In addition to the ease of glide of accumulated dislocations on the coherent TBs, TB-mediated dislocation nucleation can play an important role in mobile dislocation density. Associated with the slip transfers at TBs, a high density of interfacial defects, i.e. steps and locks, are built up [14]. These defects, on one hand, oppose the glide of TB dislocations, thereby promoting the strain hardening, as detailed below. On the other hand, they could act as dislocation sources, as observed from atomistic simulations [38] and experiments [39]; the applied high stress at the GPa level facilitates nucleation by lowering the effective energy barrier. However, further studies are needed to elucidate the relative effectiveness of TBs and GBs in generating lattice dislocations under the experimental conditions of stress and strain rate.

Furthermore, a recent TEM experiment has revealed frequent dislocation nucleation from the intersections between TBs and GBs [39]. The importance of such intersections in mobile dislocation density can be appreciated by noting the two very different characteristic structural length scales: the twin lamella thickness in the tens of nanometer range and the twin lamella length in the hundreds of nanometer range. While the former plays a similar role as the grain size of nanocrystals in obstructing dislocation motion, the latter provides a considerable space for dislocations to nucleate, move and accumulate on the TBs and within the twin lamellae as well.

Besides direct influences of TBs on the glide and multiplication of mobile dislocations, the effects of TBs on the evolution of mobile dislocation density can be correlated with that on the strain-hardening behavior. From Eq. (10), it can be seen that a large K value, which corresponds to a high rate of strain hardening, gives a low immobilizion parameter β. This can consequently lead to a low rate of mobile dislocation exhaustion, as indicated by Eqs. (8) and (9), and as shown in Table 1. Our previous study has demonstrated that at a given plastic strain of 2%, the strain-hardening rate in nt-15 Cu is much higher than that of nt-35 and ufg-Cu without twins [40]. The high rate of strain hardening in nt-Cu can be correlated to the processes described herein of TB-mediated dislocation multiplication and exhaustion. Essentially, TBs are much more hardenable than conventional high-angle GBs as TBs gradually lose coherence during plastic flow [3]. The limited hardenability of random GBs arises because of the boundary incoherency and the nanometer length scale in nanocrystals. Indeed, drastically diminished work hardening has been measured in nc metals with a few per cent uniform plastic strain in uniaxial tension (usually less than 3–5%) [1,6,7]. In contrast, comparing Fig. 7a and b, the initially clean TBs can be severely strained with a high density of dislocations concentrated at TBs, indicating the build up of a large amount of dislocations starting from a low level. The effective strain hardening can not only lower the rate of mobile dislocations density exhaustion, but can also help delay the onset of necking, thereby promoting the tensile ductility [5–7].

6. Summary

We have studied the twin thickness mediated plastic deformation kinetics in nt-Cu by using stress-relaxation tests. The size-dependent activation volume and mobile dislocation density are quantitatively characterized. These properties underlie the macroscopic deformation characteristics of strength, ductility and strain hardening. For nt-15 Cu (with the smallest twin thickness $\lambda = 15$ nm), the apparent activation volumes are measured to be about $20b^3$, signifying a dominant rate process of TB-mediated cross-slip of dislocations. Furthermore, we find that a H–P-type relation fits closely the experimental data of activation volume vs. twin thickness. This size-dependence is interpreted to arise from a transition of the rate-controlling mechanism from the intra-twin to twin-boundary-mediated processes with decreasing twin thickness.

Using stress-relaxation transients we obtain both the apparent and physical activation volumes, so that the contribution to the plastic strain rate of mobile dislocation density and dislocation velocity can be separated. We find that an increased twin density can lower the exhaustion rate of mobile dislocations, creating an opposite trend of twin-thickness dependent stress-relaxation rate. Of particular note is that the exhaustion rate of mobile dislocations in nt-Cu is much lower than that reported for nc metals. We attribute both the size effect and the low exhaustion rate of mobile dislocations to the increased strain hardening asso-

ciated with a high density of TBs, as well as the unique role of coherent TBs in preserving mobile dislocations. Our results demonstrate that study of the stress-relaxation process facilitates a quantitative understanding of the effects of dislocation velocity and mobile dislocation density on plastic flow in nanostructured metals, providing mechanistic insights into the optimization of strength and ductility by engineering nanoscale interfaces.

Acknowledgments

L.L. and K.L. thank NSFC (Grant Nos. 50571096, 50621091, 50725103 and 50890171), the MOST of China (Grant No. 2005CB623604). L.L., M.D. and S.S. acknowledge support from the Office of Naval Research Grant N00014-08-WR-2-0227 on "Surface Engineering and Mechanisms of Damage Evolution at Tribologically Active Surfaces". S.S. and M.D. further acknowledge support from the Advanced Materials for Micro and NanoSystems Programme and the Infectious Disease Interdisciplinary Research Group of the Singapore-MIT Alliance. T.Z. acknowledges the support by NSF Grants CMMI 0653769, 0758265 and 0825435. L.L. and T.Z. are supported by the CAS/SAFEA international partnership program for Creative Research Team.

References

[1] Koch CC, Morris DG, Lu K, Inoue A. MRS Bull 1999;24:54.
[2] Zhu YT, Liao XZ. Nat Mater 2004;3:351–90.
[3] Lu K, Lu L, Suresh S. Science 2009;324:349.
[4] Hutchinson J, Neale K. Acta Metall 1977;25:839.
[5] Hart E. Theory of tensile test. Acta Metall 1967;15:351.
[6] Zhu T, Li J, Samanta A, Kim HG, Suresh S. Proc Natl Acad Sci 2007;104:3031.
[7] Dao M, Lu L, Asaro RJ, De Hosson JTM, Ma E. Acta Mater 2007;55:4041.
[8] Meyers MA, Mishra A, Benson DJ. Prog Mater Sci 2006;51:427.
[9] Orowan E. Proc Phys Soc 1940;52:8.
[10] Caillard D, Martin JL. Thermal activated mechanisms in crystal plasticity. Amsterdam: Pergamon; 2003.
[11] Shen YF, Lu L, Lu QH, Jin ZH, Lu K. Scr Mater 2005;52:989.
[12] Lu L, Chen X, Huang X, Lu K. Science 2009;323:607.
[13] Lu L, Shen YF, Chen XH, Qian LH, Lu K. Science 2004;304:422.
[14] Lu L, Schwaiger R, Shan ZW, Dao M, Lu K, Suresh S. Acta Mater 2005;53:2169.
[15] Shen YF, Lu L, Dao M, Suresh S. Scr Mater 2006;55:319.
[16] Wang YM, Hamza AV, Ma E. Appl Phys Lett 2005;86:241917.
[17] Wang YM, Hamza AV, Ma E. Acta Mater 2006;54:2715.
[18] Dalla Torre F, Spatig P, Schaublin R, Victora M. Acta Mater 2005;53:2337.
[19] Martin JL, Lo Piccolo B, Kruml T, Bonneville J. Mater Sci Eng A 2002;322:118.
[20] Bonnentien J, Spatig P, Martin JL. Mater Res Soc Symp Proc 1995;364:369.
[21] Lu L, Dao M, Zhu T, Li J. Scr Mater 2009;60:1062.
[22] Conrad H. High strength materials. NewYork: Wiley; 1964.
[23] Zhu T, Li J, Ogata S, Yip S. MRS Bull 2009;34:167.
[24] Conrad H. Metall Mater Trans A 2004;35A:2681.
[25] Cahn JW, Nabarro FRN. Philos Mag A 2001;81:1409.
[26] Chen J, Lu L, Lu K. Scr Mater 2006;54:1913.
[27] Conrad H. Nanotechnology 2007;18:325701.
[28] Armstrong RW, Podriguez P. Philos Mag 2006;86:5787.
[29] Asaro RJ, Suresh S. Acta Mater 2005;53:3369.
[30] Dao M, Lu L, Shen Y, Suresh S. Acta Mater 2006:54.
[31] Jerusalem A, Dao M, Suresh S, Radovitzky R. Acta Mater 2008;56:4647.
[32] Koch CC. Scr Mater 2003;49:657.
[33] Mahajan S, Barry DE, Eyre BL. Philos Mag 1970;21:43.
[34] Mahajan S, Chin GY. Acta Metall 1973;21:173.
[35] Christian JW, Mahajan S. Prog Mater Sci 1995;39:1.
[36] Jin ZH, Gumbsch P, Albe K, Ma E, Lu K, Gleiter H, Hahn H. Acta Mater 2008;56:1126.
[37] Jin ZH, Gumbsch P, Ma E, Albe K, Lu K, Hahn H, Gleiter H. Scr Mater 2006;54:1163.
[38] Konopka K, Mizera J, Wyrzykowski JW. J Mater Process Tech 2000;99:255.
[39] Wang Y, Sui M, Ma E. Philos Mag Lett 2007;87:935.
[40] Chen XH, Lu L. Scr Mater 2007;57:133.